Article

Cell Reports

IL-4 Induces Metallothionein 3- and SLC30A4-Dependent Increase in Intracellular Zn^{2+} that Promotes Pathogen Persistence in Macrophages

Graphical Abstract

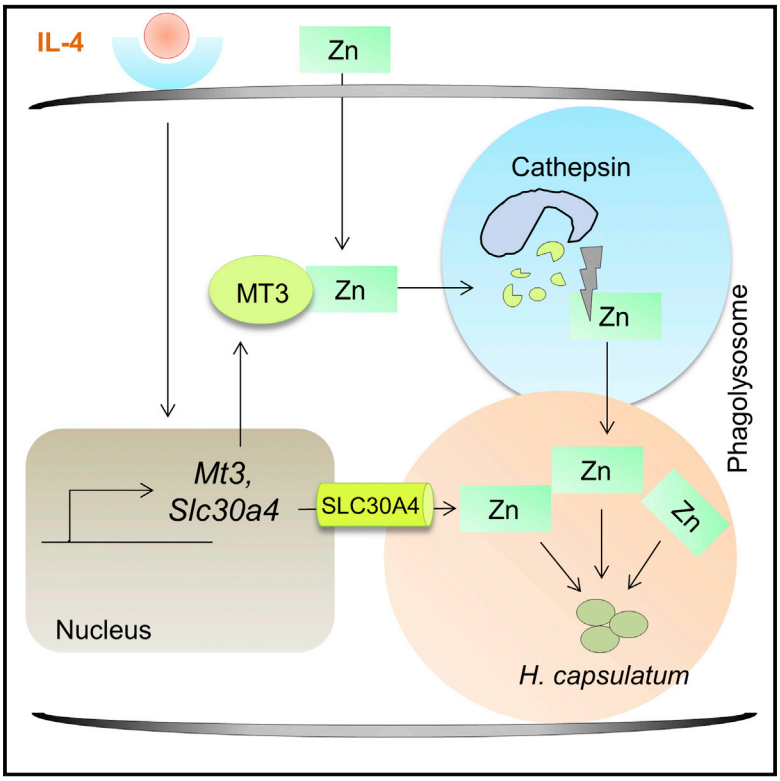

Highlights

- IL-4 and IL-13 increase the intracellular labile Zn^{2+} pool in macrophages
- MT3 and SLC30A4 shape the exchangeable Zn^{2+} reservoir in M2 macrophages
- MT3 promotes zinc uptake by an invading intracellular pathogen

Authors

Kavitha Subramanian Vignesh, Julio A. Landero Figueroa, Aleksey Porollo, Senad Divanovic, Joseph A. Caruso, George S. Deepe, Jr.

Correspondence

george.deepe@uc.edu

In Brief

M2 macrophages poorly combat intracellular infection. Vignesh et al. show that M2-polarizing signals rewire the zinc regulatory machinery in macrophages via metallothionein 3 and the zinc transporter SLC30A4. These signals result in a labile zinc-rich environment that can be exploited by intracellular pathogens for zinc nourishment and survival.

Subramanian Vignesh et al., 2016, Cell Reports *16*, 3232–3246
September 20, 2016
http://dx.doi.org/10.1016/j.celrep.2016.08.057

OPEN ACCESS
CellPress

Cell Reports
Article

IL-4 Induces Metallothionein 3- and SLC30A4-Dependent Increase in Intracellular Zn^{2+} that Promotes Pathogen Persistence in Macrophages

Kavitha Subramanian Vignesh,[1,6] Julio A. Landero Figueroa,[2,6] Aleksey Porollo,[3] Senad Divanovic,[4] Joseph A. Caruso,[2] and George S. Deepe, Jr.[1,5,7,*]

[1]Division of Infectious Diseases, College of Medicine, University of Cincinnati, Cincinnati, OH 45267, USA
[2]University of Cincinnati/Agilent Technologies Metallomics Center of the Americas, Department of Chemistry, University of Cincinnati, Cincinnati, OH 45221, USA
[3]Center for Autoimmune Genomics and Etiology and Division of Biomedical Informatics
[4]Division of Immunobiology
Cincinnati Children's Hospital Medical Center, Cincinnati, OH 45229, USA
[5]Veterans Affairs Hospital, Cincinnati, OH 45220, USA
[6]Co-first author
[7]Lead Contact
*Correspondence: george.deepe@uc.edu
http://dx.doi.org/10.1016/j.celrep.2016.08.057

SUMMARY

Alternative activation of macrophages promotes wound healing but weakens antimicrobial defenses against intracellular pathogens. The mechanisms that suppress macrophage function to create a favorable environment for pathogen growth remain elusive. We show that interleukin (IL)-4 triggers a metallothionein 3 (MT3)- and Zn exporter SLC30A4-dependent increase in the labile Zn^{2+} stores in macrophages and that intracellular pathogens can exploit this increase in Zn to survive. IL-4 regulates this pathway by shuttling extracellular Zn into macrophages and by activating cathepsins that act on MT3 to release bound Zn. We show that IL-4 can modulate Zn homeostasis in both human monocytes and mice. In vivo, MT3 can repress macrophage function in an M2-polarizing environment to promote pathogen persistence. Thus, MT3 and SLC30A4 dictate the size of the labile Zn^{2+} pool and promote the survival of a prototypical intracellular pathogen in M2 macrophages.

INTRODUCTION

Macrophage polarization involves intricate programing pathways that generate phenotypically and functionally distinct subsets. Alternative activating signals such as interleukin (IL)-4 and IL-13 differentiate macrophages to an M2 phenotype, with characteristics distinct from M1 or classically activated macrophages. IL-4-polarized M2 macrophages will be referred to herein as M2(IL-4) in accord with a recently published perspective regarding macrophage nomenclature (Murray et al., 2014). M2(IL-4) macrophages are anti-inflammatory and inhibit host defenses against intracellular pathogens (Mosser, 2003). The mechanisms that augment permissiveness of M2(IL-4) macrophages to intracellular pathogens and promote their survival remain obscure.

M2 macrophages primarily regulate type 2 immune responses and fight parasite infections but exert poor intracellular antimicrobial defense mechanisms. Exaggerated IL-4 and IL-13 production subverts macrophage immunity to a variety of intracellular pathogens. For example, *Histoplasma capsulatum*, *Cryptococcus neoformans*, and *Mycobacterium tuberculosis* establish a protective niche within the permissive environment of M2 macrophages and evade immunological recognition (Kahnert et al., 2006; Leopold Wager and Wormley, 2014; Verma et al., 2015). The expression of arginase-1 induced by IL-4 disrupts generation of nitric oxide (NO), a mechanism considered to diminish macrophage resistance to pathogens susceptible to this radical (Mosser, 2003). The prevailing theory of Fe metabolism by M2 macrophages has been used to explain poor killing of intracellular pathogens. IL-4 and IL-13 upregulate the transferrin receptor, facilitating iron uptake, and increase translation of the Fe storage protein, ferritin (Teigelkamp et al., 1991). Limitation of Fe by proinflammatory macrophages is recognized as an efficient nutritional-withholding mechanism to control infection (Hood and Skaar, 2012). However, the converse regulation of Fe in M2 macrophages favors the hypothesis of attenuated intracellular defense mechanisms in these cells. For example, infection of M2 macrophages with *M. tuberculosis* exposes intracellular bacteria to increased iron availability via high surface expression of the transferrin receptor (Kahnert et al., 2006).

Metal homeostasis and regulation in the immune system facilitates optimal development and function of myeloid and lymphoid populations. Zn-binding proteins constitute 10% of the mammalian proteome and mediate catalytic, structural, and signaling roles in cellular processes. Zn deficiency

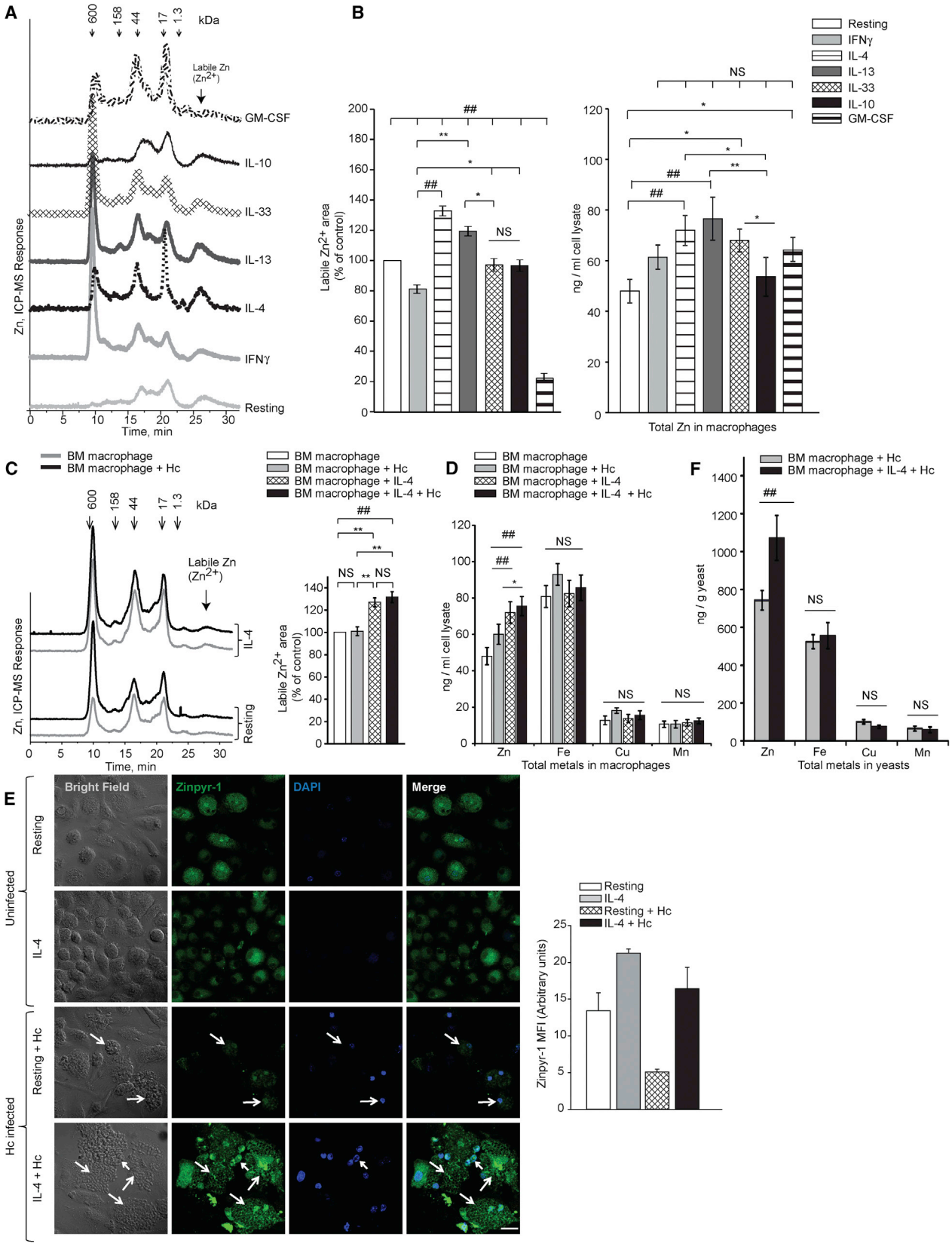

(legend on next page)

resulting from malnutrition, dysregulated homeostasis, or genetic disorders profoundly increases susceptibility to viral and bacterial infections (Haase and Rink, 2014). Zn ions act as signaling molecules and control various immunological processes in response to cytokine activation or microbial invasion.

Metal deprivation operates as a defense mechanism against infections. Zn is critical for survival of invading pathogens within the host. Neutrophils sequester extracellular Zn through calprotectin to arrest growth of *Candida albicans* and *Staphylococcus aureus* (Hood and Skaar, 2012). Physiological Zn homeostasis is regulated by metallothioneins (MTs) and spatiotemporal regulation of Zn importers (ZIPs; SLC39A) that import extracellular and intra-organelle Zn into the cytosol and exporters (ZnTs; SLC30A) that channel cytosolic Zn into extracellular space and organelles. MTs are induced by stress stimuli such as oxidative damage or microbial infection and tightly control intracellular labile Zn (Zn^{2+}). MTs are ~70% homologous, but MT3 that is highly expressed in the brain possesses two structural properties that set it apart from other MTs, a TCPCP motif and an additional hexapeptide insertion away from the metal-binding cluster. These differences impart an unstable and open conformation that alters dynamic interaction of the Zn-thiolate cluster of MT3 with the surrounding environment (Ding et al., 2010). Thus, while MT1 and MT2 exert strong metal chelating properties, the MT3 isoform has been associated with Zn^{2+} release upon stimulation (Lee and Koh, 2010). Thus far, an immunological role for MT3 has remained unknown.

We showed that macrophages activated by granulocyte macrophage-colony stimulating factor (GM-CSF) sequester intracellular labile Zn^{2+} specifically through the synthesis of MT1 and MT2. This mechanism induces a state of labile Zn^{2+} deprivation that boosts superoxide defenses and arrests intracellular survival of the fungal pathogen, *H. capsulatum*. GM-CSF stimulation reduces total macrophage Fe but does not affect acquisition of the metal by yeasts (Subramanian Vignesh et al., 2013a). Herein, we establish a regulatory pathway specifically governed by MT3 and the Zn exporter SLC30A4 (ZnT4) that expends host intracellular Zn^{2+}, but not iron resources, for metal nourishment of an invading pathogen. The fundamental control of host-pathogen interactions by MT3 and SLC30A4 uncovered herein significantly influence our current knowledge concerning phagocyte biology at steady state and in disease.

RESULTS

M2-Polarizing Agents Alter Macrophage Zn Homeostasis and Promote Pathogen Zn Acquisition

Proinflammatory activation of bone marrow macrophages by GM-CSF triggers Zn sequestration, thereby constricting the intracellular labile Zn^{2+} pool (Subramanian Vignesh et al., 2013a). To examine the specificity of pro- and anti-inflammatory signals in altering Zn homeostasis, macrophages were exposed to interferon γ (IFNγ), GM-CSF, IL-4, IL-13, IL-33, or IL-10. We confirmed the activity of these cytokines on macrophages (Figure S1A). We analyzed the impact of these polarizing signals on Zn distribution across various molecular mass fractions in macrophages. Size exclusion chromatography- inductively coupled plasma-mass spectrometry (SEC-ICP-MS-MS) revealed that only IL-4 and IL-13 increased intracellular labile Zn^{2+} (>23 min in the chromatogram) by 31% ± 5% and 20% ± 6%, respectively, accompanied by a 50% ± 6% increase in total macrophage Zn compared with resting cells. In agreement with our previous finding, GM-CSF constricted the intracellular labile Zn^{2+} pool (Subramanian Vignesh et al., 2013a). This effect, albeit modest, also was observed with IFNγ (Figures 1A and 1B). Zn signals act parallel to cytosolic changes in labile Ca (Ca^{2+}) in monocytes (Haase et al., 2008). Thus, we asked if M2 polarization by IL-4 altered Ca^{2+} flux in parallel. At 24 hr, when labile Zn^{2+} was elevated, the Ca^{2+} pool was increased by 18% and 24% in IL-4- and IL-13-treated macrophages, respectively (Figure S1B). Thus, M2-polarizing signals modulate Zn homeostasis to expand the intracellular labile Zn^{2+} reservoir.

M2 macrophages facilitate parasite clearance but harbor a favorable environment for the persistence of intracellular pathogens (Mosser and Edwards, 2008). *H. capsulatum* infects and replicates within macrophages prior to proinflammatory activation by GM-CSF or IFNγ (Allendoerfer and Deepe, 1997). We queried whether the fungus exploited an M2-polarized state to acquire Zn from the host. As the intracellular Zn response was similar with IL-4 and IL-13, we focused on IL-4 to generate M2(IL-4) macrophages. Resting and M2(IL-4) macrophages were infected with *H. capsulatum* yeasts. Similar to the elevated labile Zn^{2+} pool observed in uninfected M2(IL-4) macrophages, IL-4 augmented this pool upon *H. capsulatum* infection at 24 hr compared with resting cells (Figure 1C). Unlike GM-CSF that elicits a large influx of total Zn in infected macrophages (Subramanian Vignesh et al., 2013a), IL-4 modestly increased total Zn, but not Fe, Cu, or Mn (Figure 1D). Next, we determined whether

Figure 1. M2 Signals Elevate Labile Zn^{2+} and Promote Pathogen Zn Uptake

(A) SEC-ICP-MS-MS in response to cytokines, y axis, off-set Zn signal.

(B) Labile Zn^{2+} area (after 23 min) (left) and total Zn from SEC chromatograms compared with resting control, three (resting, GM-CSF, and IL-4) and two (IFNγ, IL-13, IL-33, and IL-10) experiments. Data represent mean ± SD.

(C) SEC-ICP-MS-MS of resting and M2 macrophages 24 hr post-*H. capsulatum* (Hc) infection, percentage quantification of labile Zn^{2+} area (after 23 min) compared with resting cells. Data represent mean ± SD.

(D) ICP-MS-MS of total Zn, Fe, Cu, and Mn in macrophage lysates 24 hr post-IL-4 stimulation and infection; y axis values are metal concentration per milliliter lysate from 2.5×10^6 macrophages, three independent experiments. Data represent mean ± SD.

(E) Zinpyr-1-stained macrophages 24 hr post-infection. Arrows indicate Zinpyr-1 staining in infected resting and M2 macrophages showing cytosolic and nuclear distribution. The scale bar represents 20 μm. Representative images from two experiments. The bar graph shows quantification of Zinpyr-1 fluorescence from 2 fields for uninfected and 9–11 fields for infected cells obtained in a single experiment, mean ± SEM.

(F) ICP-MS-MS of total metal in Hc from macrophages 24 hr post-infection, three experiments; mean ± SD.

See also Figure S1.

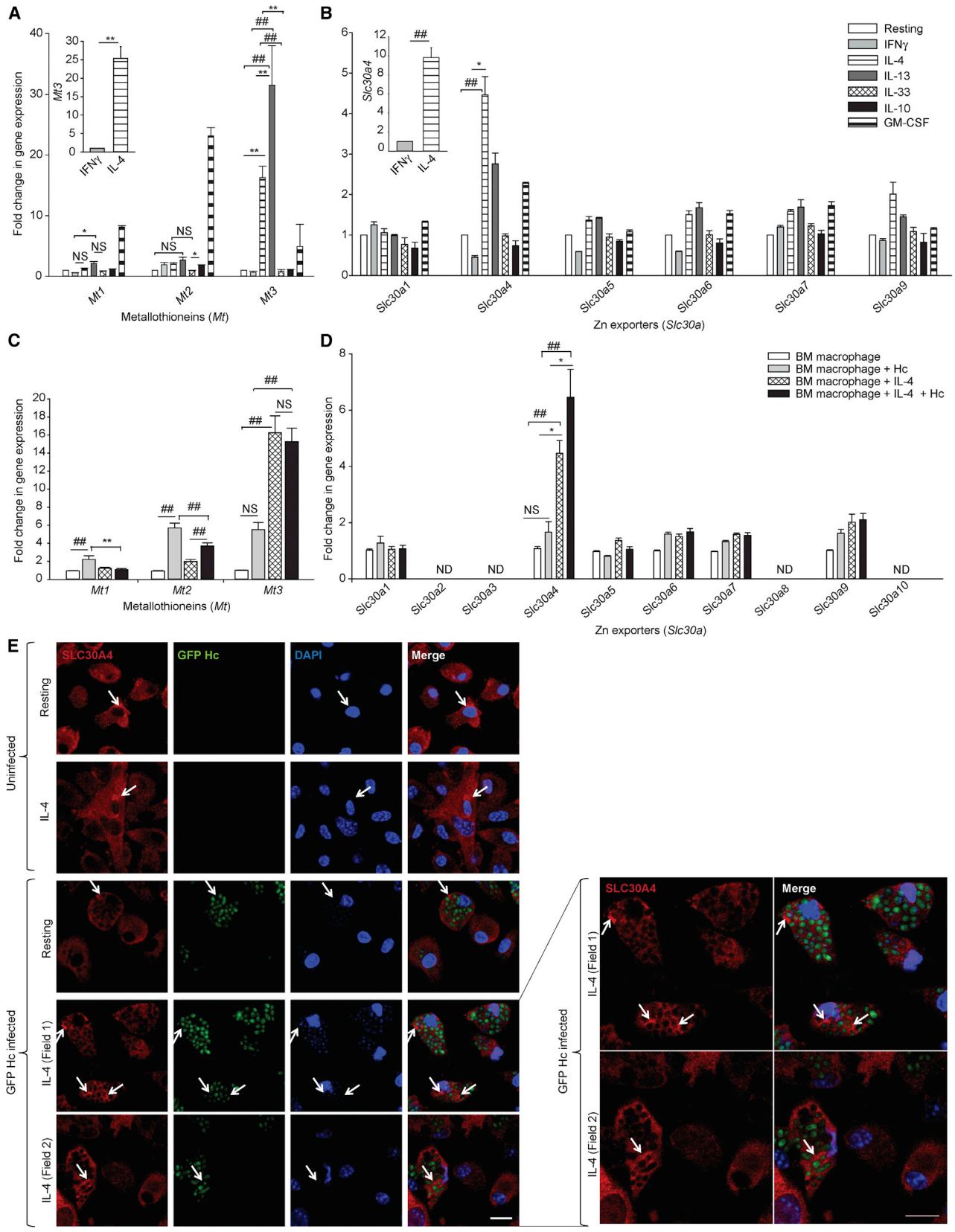

(legend on next page)

IL-4 dynamically modulated the labile Zn^{2+} stores during infection. Resting and M2(IL-4) macrophages were infected with yeasts and harvested at 0, 9, 12, and 24 hr. M2(IL-4) macrophages exhibited a gradual increase in the labile Zn^{2+} pool in a time-dependent manner (Figure S1C). We previously showed that the Zn probe Zinpyr-1 binds labile Zn^{2+} in macrophages (Figueroa et al., 2014). To ensure that changes in the labile Zn^{2+} pool observed by SEC-ICP-MS-MS after cell lysis could also be observed in intact macrophages, we stained live macrophage cultures with Zinpyr-1. In agreement with SEC-ICP-MS-MS analysis, uninfected and infected M2(IL-4) macrophages exhibited enhanced labile Zn^{2+} staining compared with resting cells. The Zinpyr-1 signal was mostly cytosolic in uninfected M2(IL-4) macrophages, but upon infection, nuclear and cytosolic staining were observed (Figure 1E). Treatment with a Zn chelator reversed Zinpyr-1 staining, confirming that the fluorescence signal resulted from Zn binding (Figure S1D). Next, we assessed metal content of intracellular yeasts by harvesting them from resting and M2(IL-4) macrophages 24 hr post-infection. Fungi thriving in M2(IL-4) macrophages contained more Zn, but not Fe, Cu, or Mn (Figure 1F). These data reveal that elevated labile Zn^{2+} stores engender a Zn-replete state in M2(IL-4) macrophages that is permissively harnessed by fungi from the host.

M2 Polarization Induces an Upregulated MT3 and SLC30A4 Response in Macrophages

To investigate the Zn regulatory machinery specifically induced by IL-4, we generated gene expression profiles of macrophages stimulated with IFNγ, GM-CSF, IL-4, IL-13, IL-33, or IL-10, as in Figure 1A. Consistent with prior findings (Subramanian Vignesh et al., 2013a), macrophage polarization with GM-CSF, but none of the other cytokines analyzed, induced *Mt1*, *Mt2*, and Zn importer *Slc39a2* expression. IL-4 and IL-13 specifically induced *Slc30a4* and *Mt3* but not *Mt1* and *Mt2* expression compared to resting macrophages (Figures 2A, 2B, and S2A).

We asked whether changes in these Zn regulatory genes also occurred during infection. Similar to the response in uninfected cells, IL-4 enhanced the expression of *Slc30a4* and *Mt3* but not *Mt1* and *Mt2* in *H. capsulatum*-infected macrophages (Figures 2C and 2D). *Mt1* and *Mt2* were marginally but significantly ($p < 0.001$) upregulated in infected resting macrophages but downregulated in response to IL-4 (Figure 2C). The ZIPs *Slc39a2*, *Slc39a4*, and *Slc39a14* were induced only upon infection and were not specific to IL-4 stimulation (Figure S2B).

We performed proteomic analysis on uninfected resting and M2(IL-4) macrophages or those infected with *H. capsulatum* for 24 hr. SLC30A4 was detected through bottoms-up proteomic approach in infected M2(IL-4) macrophages (Table S1). Next, we determined the cellular distribution of this Zn transporter that shuttles the cytosolic Zn fraction into extracellular space or into intracellular organelles. In uninfected macrophages, SLC30A4 staining was epinuclear as well as diffuse, but upon infection, the protein appeared on the cell surface as well as on the membrane surrounding intracellular GFP^+ *H. capsulatum* yeasts (Figure 2E). To determine if SLC30A4 was on the phagolysosomal membrane of infected macrophages, we analyzed lysosomal associated membrane protein 1 (LAMP1) and SLC30A4 in resting and M2(IL-4) macrophages. SLC30A4 and LAMP1 colocalized to some degree in uninfected cells, and increased colocalization was observed upon infection, especially in M2(IL-4) macrophages (Figure S2C). These data suggest that SLC30A4 may facilitate Zn transport into phagolysosomes in macrophages harboring yeasts.

STAT6 and IRF4 Drive the MT3 and SLC30A4 Program

IL-4 alternatively activates macrophages through the signal transducer and activator of transcription factor STAT6 and interferon regulatory factor, IRF4 (El Chartouni et al., 2010). We asked if either of these factors was necessary for enhanced *Mt3* or *Slc30a4* expression. Both $Stat6^{-/-}$ and $Irf4^{-/-}$ macrophages showed impaired induction of *Mt3* and *Slc30a4* in response to IL-4 24 hr post-infection. The expression of *Irf4* was STAT6 dependent (Figures 3A and 3B). We found that *Mt3* and *Slc30a4* genes were rapidly induced 15 and 30 min post-infection in IL-4-stimulated wild-type (WT) but not $Stat6^{-/-}$ macrophages (Figure 3C). Thus, STAT6 and IRF4 govern the MT3 and SLC30A4 program in M2(IL-4) macrophages.

MT3 and SLC30A4 Elevate the Labile Zn^{2+} Pool and MT3 Promotes Pathogen Zn Uptake

We examined if *Mt3* and *Slc30a4* regulated the intracellular labile Zn^{2+} reservoir and facilitated fungal Zn accrual in M2(IL-4) macrophages. We individually silenced *Mt3* and *Slc30a4* genes using small interfering RNA (siRNA) by 91% and 80%, respectively, and silenced them in combination by 80% and 71%, respectively, in IL-4-treated macrophages (Figures 4A and 4B). MTs are cysteine rich (sulfur containing) and elute at ~21 min in the SEC chromatogram. *Mt3* silencing reduced the sulfur signal at ~21 min, indicating that this peak constituted MT3 (Figure 4C). Individual or combined silencing of *Mt3* and *Slc30a4* reduced the labile Zn^{2+} pool without significantly affecting total macrophage Zn (Figures 4D and 4E). Silencing *Mt3* or *Mt3* and *Slc30a4*, but not *Slc30a4* alone, diminished Zn uptake by

Figure 2. IL-4 Induces MT3 and SLC30A4 in Macrophages

(A and B) *Mt* and *Slc30a* expression in response to cytokines. Inset: *Mt3* and *Slc30a4* in M2(IL-4) macrophages compared with IFNγ group, *Slc30a2*, *3*, *8*, and *10* not detected, mean ± SEM, three (IFNγ, GM-CSF, IL-13, and IL-33), four to six (IL-4), and two (IL-10) experiments.

(C and D) Expression of *Mt* and *Slc30a1-10* genes in M2(IL-4) macrophages, left uninfected or infected with yeasts for 24 hr compared with resting control. ND, not detected. At least four independent experiments. Data represent mean ± SEM.

(E) Confocal images of SLC30A4 (red) in resting and M2(IL-4) macrophages left uninfected or infected for 2 hr with GFP^+ Hc, nuclear stain, DAPI, merge, overlay of three channels. Arrows point at epinuclear SLC30A4 in uninfected cells and SLC30A4 on cell surface or membranes surrounding yeasts in infected cells; two experiments. The scale bar represents 20 μm. Right: enlarged images of merge fields of infected M2 (IL-4) macrophages.

See also Figure S2.

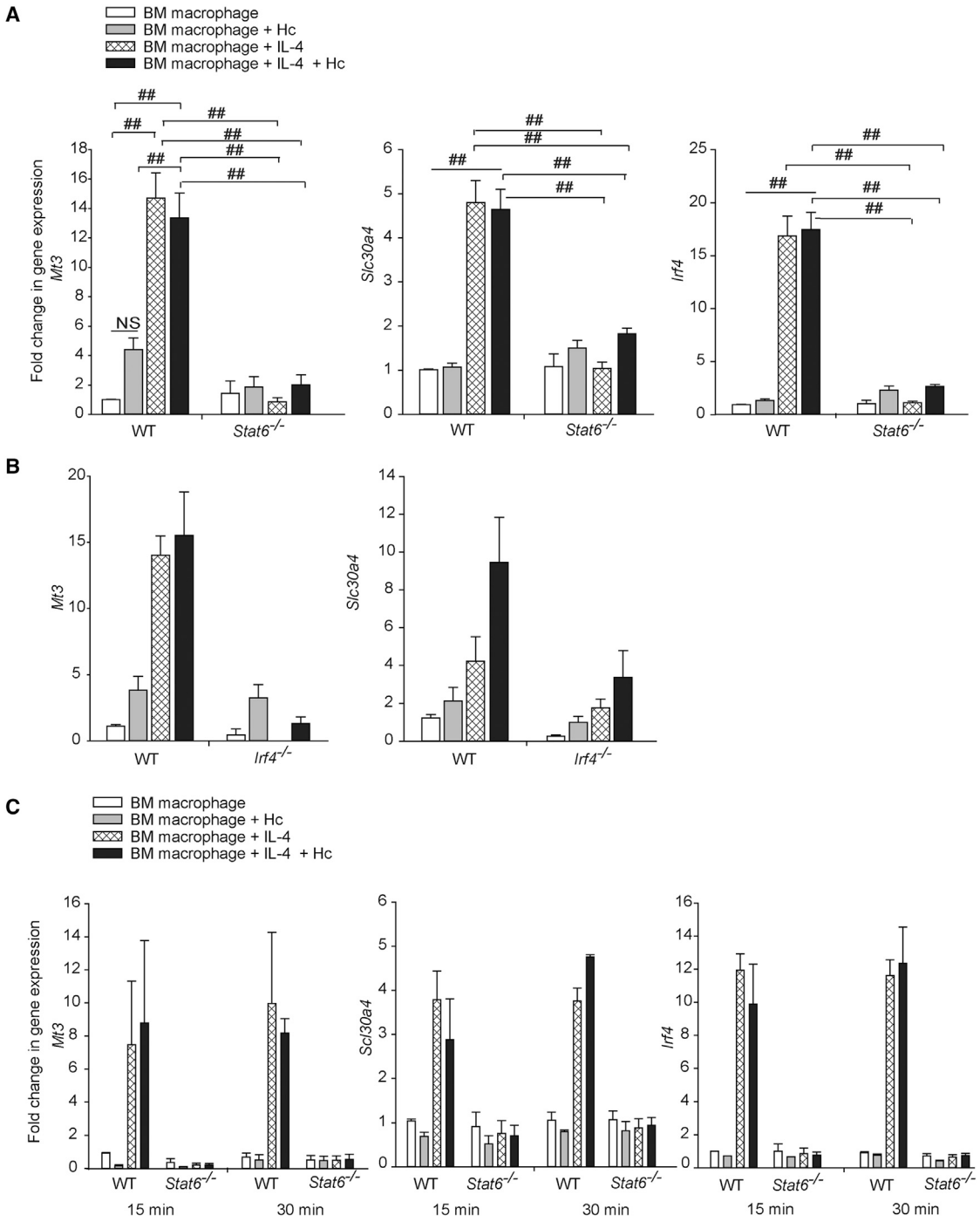

Figure 3. IL-4 Driven *Mt3* and *Slc30a4* Response Is Rapid and STAT6 and IRF4 Dependent

(A and B) *Mt3*, *Slc30a4*, and *Irf4* expression in WT and *Stat6*$^{-/-}$ macrophages, four independent experiments; and in WT and *Irf4*$^{-/-}$ macrophages 24 hr post-IL-4 stimulation and infection, two independent experiments. Data represent mean ± SEM.

(C) *Mt3*, *Slc30a4*, and *Irf4* expression in WT and *Stat6*$^{-/-}$ macrophages, 15 and 30 min post-restimulation with IL-4 and simultaneous infection with *H. capsulatum*, two independent experiments. Data are mean ± SEM.

intracellular yeasts (Figure 4F). These data indicate that MT3 and SLC30A4 shape labile Zn^{2+} homeostasis in M2(IL-4) macrophages and facilitate zinc nourishment of yeasts within the intracellular niche.

Cathepsins Regulate Expansion of the Labile Zn^{2+} Pool by MT3

The cellular proteolytic machinery controls exchangeable Zn^{2+} availability in cells. Cysteine and aspartic cathepsin proteases

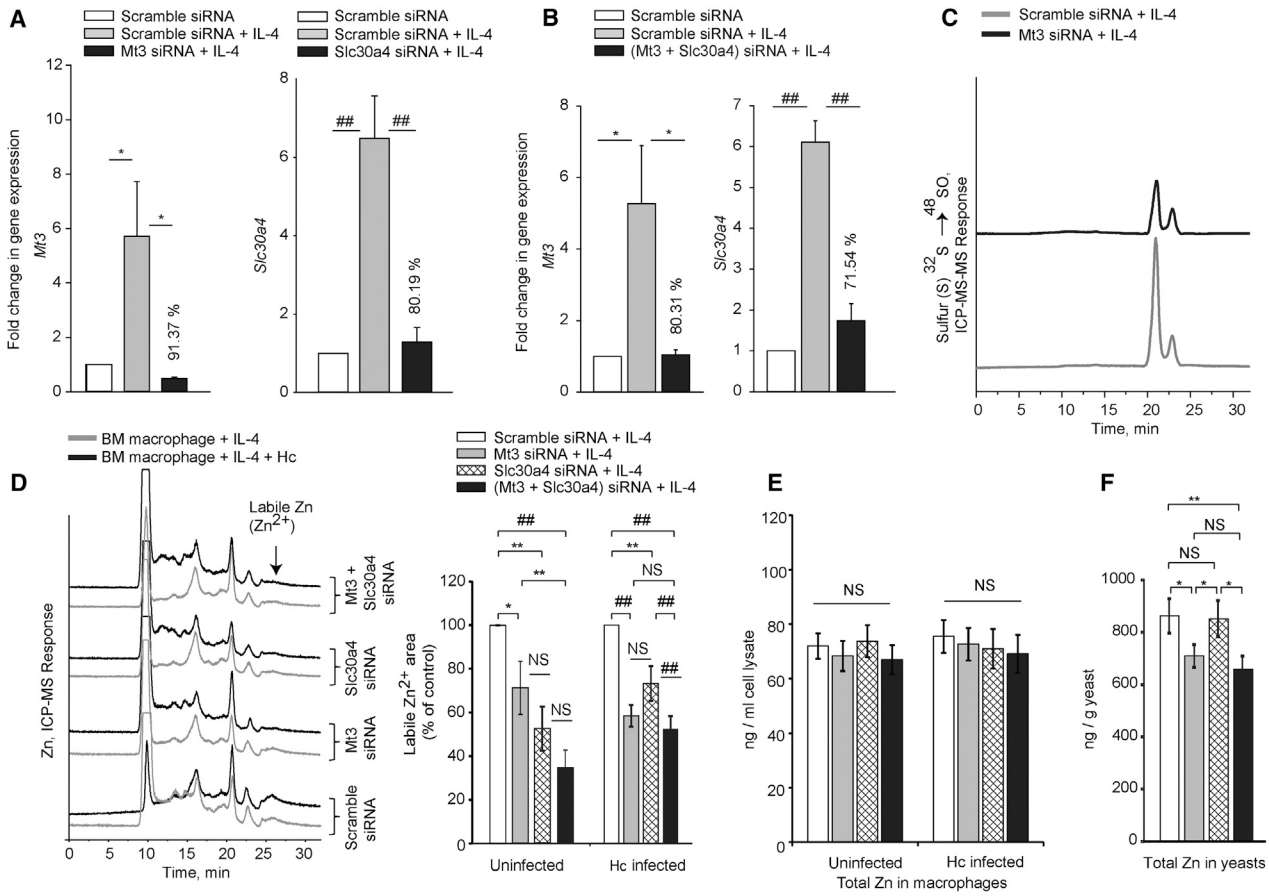

Figure 4. MT3 and SLC30A4 Augment Labile Zn^{2+} and MT3 Promotes Yeast Zn Acquisition

(A and B) *Mt3* and *Slc30a4* expression in M2(IL-4) macrophages treated individually or together with Mt3 or Slc30a4 siRNA compared with scramble siRNA control. Percentage values are decrease in gene expression compared with IL-4-treated scramble siRNA group, three experiments. Data represent mean ± SEM.

(C) SEC-ICP-MS-MS analysis of sulfur (S) signal in M2(IL-4) macrophages treated with scramble siRNA or Mt3 siRNA, three experiments.

(D) SEC-ICP-MS-MS of *Mt3*- and *Slc30a4*-silenced M2(IL-4) macrophages 24 hr post-infection, percentage quantification of labile Zn^{2+} area. Data represent mean ± SD.

(E) ICP-MS-MS analysis of total Zn in *Mt3* and *Slc30a4* siRNA or scramble siRNA treated M2(IL-4) macrophages. The y axis values are Zn concentration per milliliter lysate from 2.5 × 10^6 macrophages, three independent experiments. Data represent mean ± SD.

(F) Total Zn in Hc from M2(IL-4) macrophages 24 hr post-infection, three experiments, mean ± SD.

degrade MT1 and MT2 at low Zn saturation, but whether they target MT3 to release Zn is unknown (McKim et al., 1992). IL-4 increases cathepsin activity in the phagosomes of M2(IL-4) macrophages (Balce et al., 2011). To determine which cathepsins are expressed in M2(IL-4) macrophages, we performed proteomic analysis on resting and IL-4-treated macrophages left either uninfected or infected with *H. capsulatum* for 24 hr. We detected cathepsins CTSB, CTSS, and CTSD in both uninfected and infected M2(IL-4) macrophages (Table S1).

These data led us to test the hypothesis that the MT3-driven elevation in labile Zn^{2+} pool in M2(IL-4) macrophages was dependent on cathepsin activity. Inhibition of lysosomal cysteine cathepsins CTSB and CTSL or aspartic cathepsin CTSD using the chemical inhibitors ALLM or Pepstatin A, respectively, reduced intracellular labile Zn^{2+} (Figure 5A). Next, we sought a molecular approach to target CTSD, as inhibition of this cathepsin had a stronger effect on constricting labile Zn^{2+}. Silencing *Ctsd* using siRNA produced a similar decrease in the labile Zn^{2+} pool as observed in CTSD-inhibited macrophages (Figures S3A and S3B). Moreover, yeasts within cathepsin-inhibited or *Ctsd*-silenced M2(IL-4) macrophages exhibited diminished Zn amassment (Figures 5B and S3C).

We directly dissected the role of cathepsins in modulating MT3 function. Human CTSD was incubated for 3 hr with low (1 Zn), mid (3 Zn), or high (6 Zn) MT3 saturation at varying pH values simulating the cytosolic and phagolysosomal pH environment. Mid-Zn-saturated MT3 was incubated without CTSD as a control to monitor non-enzymatic degradation and Zn^{2+} release. The mixtures were analyzed by SEC-ICP-MS-MS by following sulfur and Zn signals in the MT3 peak (16 min region) and at low molecular mass region (past 23 min). CTSD degraded MT3 with low- and mid-Zn saturation but not the high-saturated form at pH 5.5 and 6.5, which is the pH range found in phagolysosomes. This was observed by a decrease in sulfur signal in the

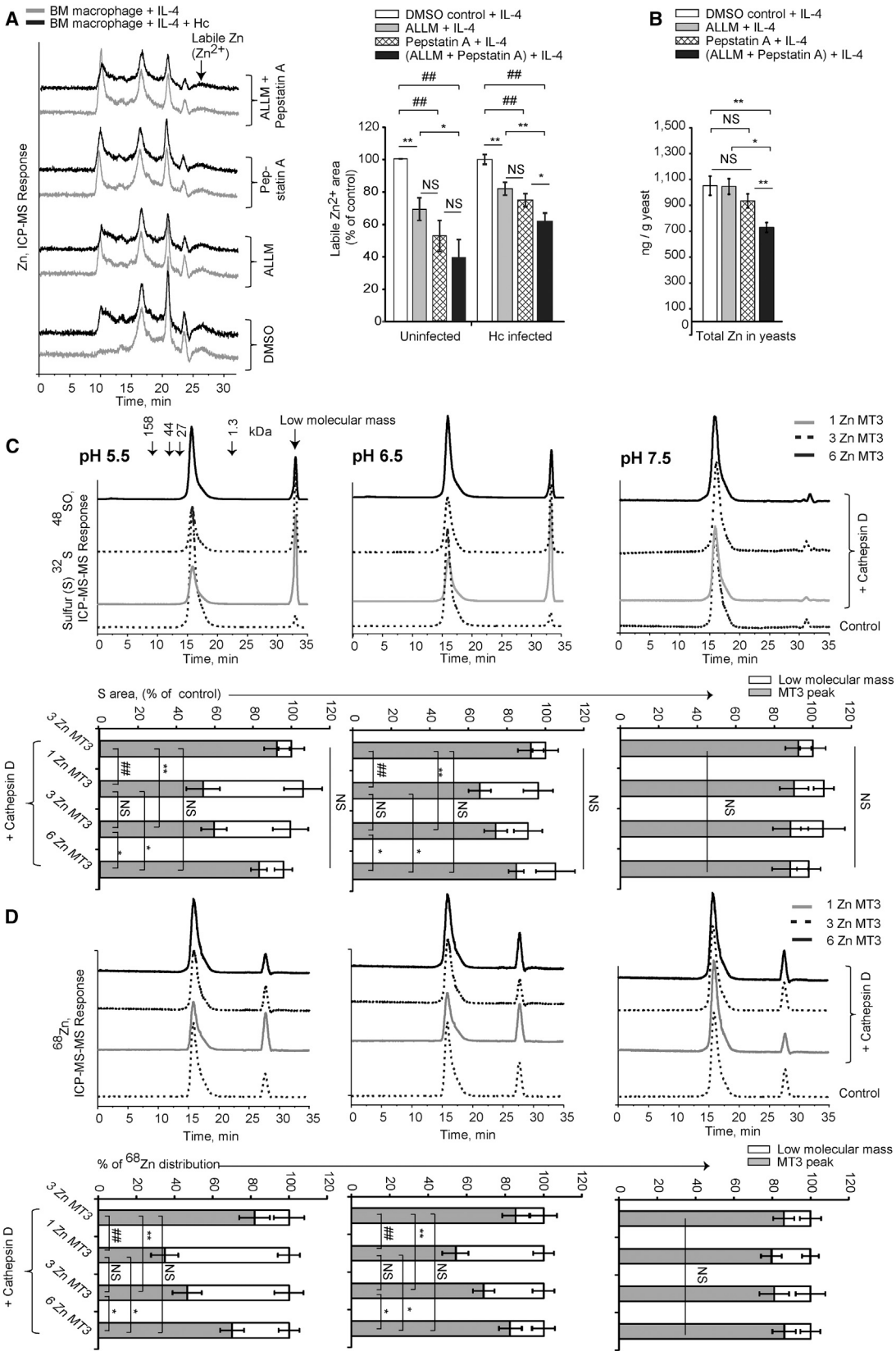

(legend on next page)

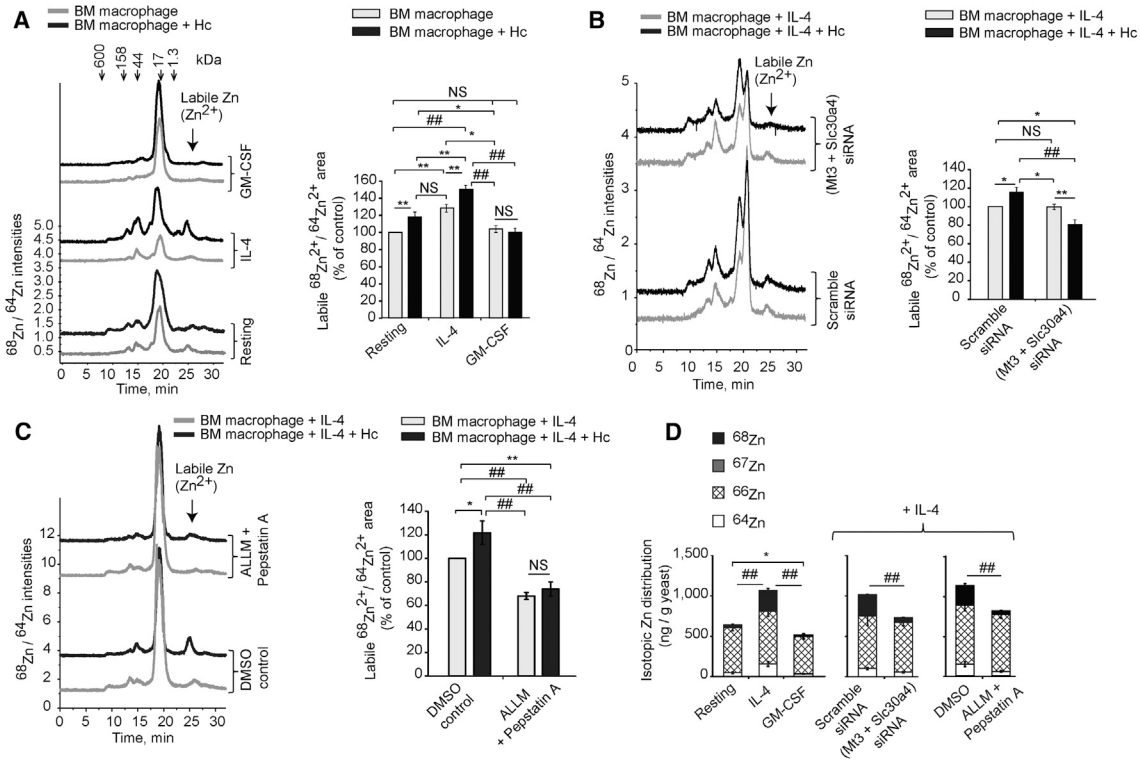

Figure 6. M2(IL-4) Macrophages Traffic Extracellular Zn into Intracellular Yeasts

(A–C) Ratio of $^{68}Zn/^{64}Zn$ intensities versus time by SEC-ICP-MS-MS analysis of ^{68}Zn and ^{64}Zn signals in (A) uninfected and infected resting IL-4- or GM-CSF-treated macrophages, (B) *Mt3* + *Slc30a4*-silenced or scramble siRNA-treated M2(IL-4) macrophages; (C) cathepsin-inhibited or DMSO-treated M2(IL-4) macrophages. Bar graphs, percentage quantification of labile Zn^{2+} area (after 23 min) compared with resting cells in (A), scramble siRNA-treated M2(IL-4) macrophages in (B), and DMSO-treated M2(IL-4) macrophages in (C). Three experiments, offset y axis of chromatograms. Data represent mean ± SD.

(D) Isotope distribution of total Zn in yeasts recovered from macrophages, three experiments, mean ± SD.

See also Figure S4.

MT3 region under these conditions (Figure 5C). Accordingly, CTSD induced Zn redistribution between the two regions of the chromatogram by releasing the metal from low- and mid-Zn-saturated MT3 and correspondingly increasing the labile Zn^{2+} signal (Figure 5D). Collectively, these data reveal that MT3-mediated control of intracellular labile Zn^{2+} in macrophages and the access gained by invading yeasts to the Zn^{2+} reservoir is potentiated by cathepsin activity.

Extracellular Zn^{2+} Trafficking Shapes the Labile Zn^{2+} Pool of M2(IL-4) Macrophages

Zn restriction is a defense strategy against intracellular infections (Subramanian Vignesh and Deepe, 2016). To further understand how M2(IL-4) macrophages modulated Zn homeostasis, we sought the source of the macrophage labile Zn^{2+} pool and Zn amassed by fungi using double isotope dilution analysis with ^{68}Zn and ^{66}Zn isotopes. We prepared RPMI and yeast growth media predominantly containing ^{68}Zn and ^{66}Zn, respectively (Figures S4A and S4B). Macrophages were rested or polarized using IL-4 in ^{68}Zn media and infected with ^{66}Zn-enriched yeasts. Zn flux in macrophages and intracellular yeasts was monitored by alterations in intracellular $^{68}Zn/^{64}Zn$ and $^{66}Zn/^{64}Zn$ ratios. Labile Zn^{2+} area was measured past 23 min in the SEC chromatogram and expressed as a ratio of $^{68}Zn^{2+}/^{64}Zn^{2+}$. M2(IL-4) polarization amplified the ratio of labile $^{68}Zn^{2+}/^{64}Zn^{2+}$ compared to resting and GM-CSF-activated macrophages (Figure 6A). Silencing *Mt3* and *Slc30a4* or inhibition of cathepsins abrogated the increase in labile $^{68}Zn^{2+}/^{64}Zn^{2+}$ (Figures 6B and 6C). Thus,

Figure 5. Cathepsins Degrade MT3 to Release Labile Zn^{2+}

(A) SEC-ICP-MS-MS of M2(IL-4) macrophages treated with cathepsin inhibitors, percentage quantification of labile Zn^{2+} area (after 23 min).

(B) Total Zn in Hc from macrophages 24 hr post-infection, three experiments.

(C) SEC-ICP-MS-MS MT3 degradation by CTSD measured as decrease in sulfur (S) signal in MT3 peak (16 min region) and corresponding S increase at low molecular mass at varying pH and ^{68}Zn MT3 saturation forms. Bar graphs are S in MT3 peak and low molecular mass, three experiments.

(D) SEC-ICP-MS-MS of $^{68}Zn^{2+}$ release measured as decrease in MT3-^{68}Zn (16 min region) and corresponding increase in labile $^{68}Zn^{2+}$ signal at low molecular mass. Bar graphs are relative ^{68}Zn distribution between MT3 peak and low molecular mass, representative of three experiments, mean ± SD, y axis of chromatograms, offset S and Zn signals.

Data represent mean ± SD. See also Figure S3.

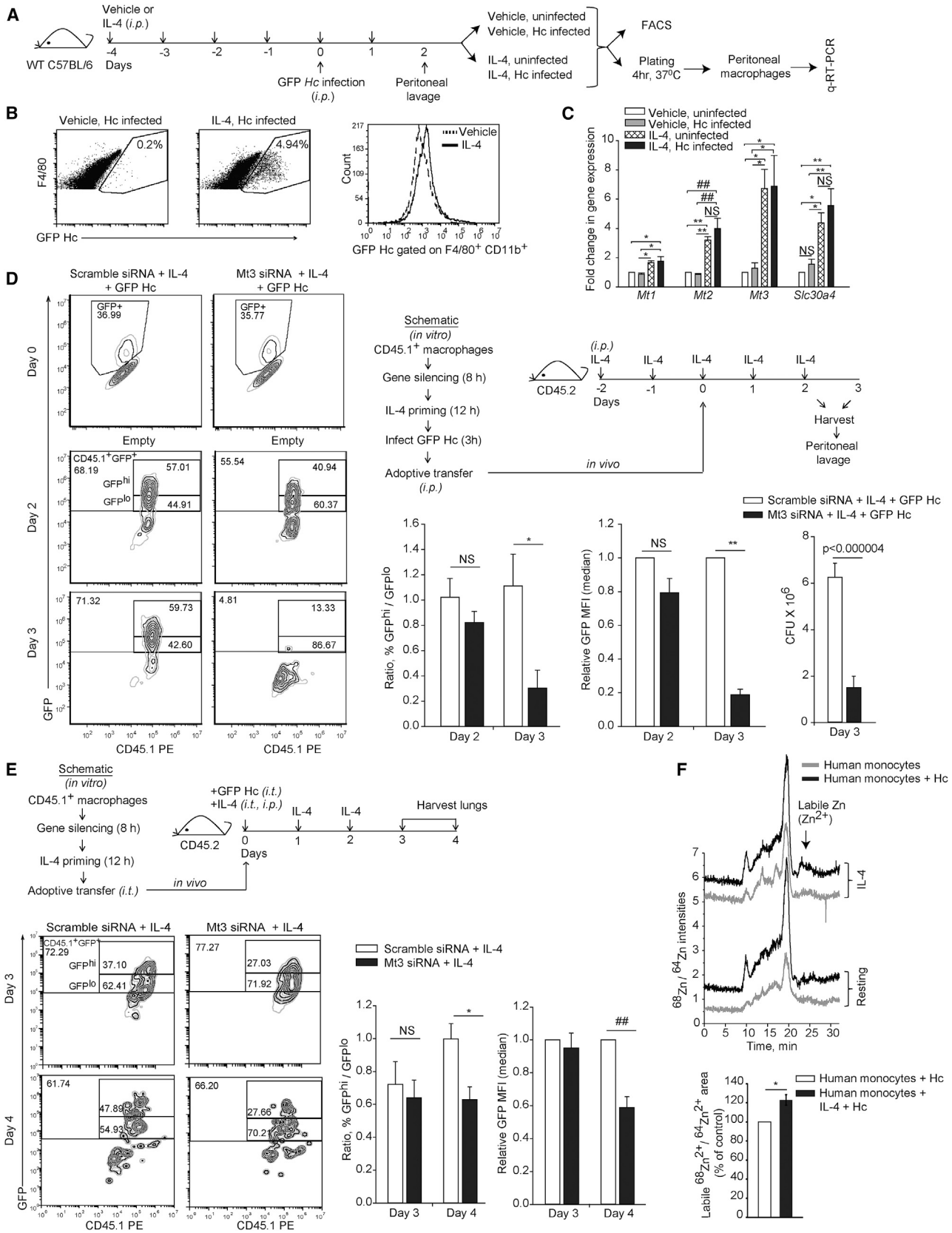

(legend on next page)

M2(IL-4) macrophages mobilized labile Zn^{2+} from the extracellular environment. While GM-CSF restricted fungal accrual of ^{68}Zn from the host, yeasts thriving within M2(IL-4) macrophages acquired greater ^{68}Zn ($p < 0.001$). Fungal uptake of host ^{68}Zn was impaired in *Mt3* and *Slc30a4*-silenced or cathepsin-inhibited M2(IL-4) macrophages (Figure 6D). In contrast to polarization by IL-4, GM-CSF constricted labile $^{68}Zn^{2+}/^{64}Zn^{2+}$ in macrophages and deprived yeast ^{66}Zn by sequestration through MTs (Figure S4C). These data are consistent with our prior finding that MTs sequester the free Zn^{2+} pool and inhibit Zn uptake by intracellular yeasts in GM-CSF-activated macrophages (Subramanian Vignesh et al., 2013a). Because GM-CSF restricts Zn through MT1 and MT2, we examined if the rise in labile Zn^{2+} in M2(IL-4) macrophages was independent of MT1 and MT2 but depended on MT3. IL-4 induced *Mt3* and elevated labile $^{68}Zn^{2+}/^{64}Zn^{2+}$ in *Mt1* and *Mt2* silenced cells similar to control M2(IL-4) macrophages, indicating that expansion of the labile Zn^{2+} reservoir was specifically driven by MT3 (Figures S4D and S4E).

We investigated the mechanism of Zn import into macrophages in response to IL-4. SLC39A2 regulates Zn influx in GM-CSF-activated proinflammatory macrophages (Subramanian Vignesh et al., 2013a). Silencing *Slc39a2* decreased total $^{68}Zn/^{64}Zn$ area by 13% ± 3% in M2(IL-4) macrophages (Figure S4F). These data reveal that the SLC39A2 importer contributes to, but does not completely regulate Zn import in M2(IL-4) macrophages.

M2 Polarization Modulates Zn Homeostasis and Fungal Survival In Vivo and in Human Monocytes

To establish the physiological relevance of our findings in vivo, we used two mouse models. We administered IL-4 to mice and intraperitoneally (i.p.) infected them with GFP^+ yeasts (Figure 7A). IL-4 increased the fungal burden as assessed by an elevation in the percentage GFP^+ macrophages and GFP mean fluorescence intensity (MFI) (Figures 7B and S5A). IL-4 induced *Mt3* and *Slc30a4* expression in macrophages in vivo, while *Mt1* and *Mt2* were moderately altered (Figure 7C). The chemokine receptor CCR2 suppresses type 2 immunity during fungal infection. Mice deficient in CCR2 exhibit decreased antifungal resistance and elevated fungal burden due to an exaggerated IL-4 response (Szymczak and Deepe, 2009). We asked if macrophages from infected $Ccr2^{-/-}$ mice exhibited changes in expression of *Mt3* and *Slc30a4* genes. We intranasally (i.n.) infected WT and $Ccr2^{-/-}$ mice with *H. capsulatum* yeasts and sorted $F4/80^+CD11b^+$ macrophages from the lungs 7 days post-infection. Macrophages recovered from $Ccr2^{-/-}$ mouse lungs strongly elevated *Mt3* and showed a trend toward enhanced *Slc30a4* expression in vivo (Figure S5B). Thus, M2-polarizing signals induce MT3 and SLC30A4 in macrophages in vivo.

Next, we investigated the role of MT3 in yeast growth in M2(IL-4) macrophages. Because MT3 had an impact on yeast Zn acquisition, we focused on this gene for assessing fungal survival. We polarized macrophages with IL-4 and then exposed them to IFNγ, followed by infection with *H. capsulatum* in vitro. IL-4 promoted yeast survival in IFNγ-treated macrophages, but this effect was attenuated when *Mt3* was silenced (Figure S5C). These cells displayed similar CD11b expression and phagocytic ability, indicating that MT3 did not affect fungal recognition and uptake (Figure S5D). Next, we queried if a lack of MT3 improved fungal clearance in vivo. We primed MT3-deficient $CD45.1^+$ macrophages with IL-4, infected them with GFP^+ yeasts in vitro, and adoptively transferred them in vivo into CD45.2 mice that received IL-4 i.p. (Figure 7D, schematic). MT3-deficient macrophages recovered by peritoneal lavage exhibited a decreased proportion of GFP^{hi} cells and GFP MFI in vivo after 2 days and cleared yeasts 3 days post-infection. To examine whether the GFP signal correlated with fungal burden, we cultured peritoneal exudates from these mice. Yeast survival was attenuated in mice that received MT3-deficient macrophages (Figure 7D). We further investigated fungal clearance by these cells using a model of pulmonary infection. We adoptively transferred *Mt3*-silenced IL-4-treated $CD45.1^+$ macrophages into lungs of CD45.2 mice, administered IL-4, and challenged them with GFP^+ yeasts in vivo (Figure 7E, schematic). *Mt3*-silenced $CD45.1^+$ macrophages exhibited a reduction in both, proportion of GFP^{hi} cells, and GFP MFI 4 days post-infection (Figure 7E). These data indicate that the lack of MT3 curtailed fungal survival in macrophages in vivo.

Next, we queried whether IL-4 regulated Zn homeostasis in human monocytes. Because humans have 17 MT isoforms, unlike 4 MTs in mice (Li and Maret, 2008), we directly assessed

Figure 7. M2 Signals Shape Zn Homeostasis In Vivo and in Human Monocytes

(A) Schematic, mice treated with 500 ng IL-4 and infected with GFP Hc i.p.

(B) Percentage GFP infected gated on $F4/80^+CD11b^+$ cells, histogram.

(C) Gene expression in peritoneal macrophages from IL-4-treated mice compared with vehicle, n = 4 mice per group. Data represent mean ± SEM.

(D) Schematic, $CD45.1^+$ macrophages treated with scramble or Mt3 siRNA for 8 hr, primed with 10 ng/ml IL-4 for 12 hr, and infected with 4×10^6 GFP^+ Hc per 5×10^6 macrophages (0.8 MOI) for 3 hr in vitro and 5×10^6 macrophages were transferred i.p. per mouse. IL-4 (500 ng) was given i.p. on indicated days, and $CD45.1^+$ cells were recovered by peritoneal lavage. Left: contour plots of percentage GFP^+ macrophages on day 0 (before transfer) and percentage $CD45.1^+GFP^+$ (black gate), gated on $F4/80^+CD11b^+$ on days 2 and 3 post-infection. Inset: percentage GFP^{hi} and GFP^{lo} gated on $CD45.1^+GFP^+$, ratio of percentage GFP^{hi}/GFP^{lo} and total relative GFP MFI in $CD45.1^+GFP^+$ gate, n = 3 (day 2), n = 5 (day 3), peritoneal exudate CFUs. Data represent mean ± SEM.

(E) Schematic, siRNA treated $CD45.1^+$ cells were primed with 10 ng/ml IL-4 in vitro; 2.5×10^6 $CD45.1^+$ cells, 2×10^6 GFP^+ Hc and IL-4 (250 ng) transferred i.t. into CD45.2 mice, and IL-4 (250 ng i.p. and 250 ng i.t.) were given on days 0, 1, and 2; lungs were harvested on days 3 and 4. Contour plots of percentage $CD45.1^+GFP^+$ (black gate), gated on $F4/80^+CD11b^+$. Inset: % GFP^{hi} and GFP^{lo} in $CD45.1^+GFP^+$ gate, ratio of percentage GFP^{hi}/GFP^{lo} and relative GFP MFI (median) in $CD45.1^+GFP^+$ gate, n = 4 (day 3), n = 5 (day 4), mean ± SEM.

(F) Ratio of $^{68}Zn/^{64}Zn$ intensities by SEC-ICP-MS-MS of human monocytes cultured in ^{68}Zn RPMI and infected, bar graph, quantification of labile $^{68}Zn^{2+}/^{64}Zn^{2+}$ area in infected monocytes, three donors, mean ± SD.

See also Figure S5.

the impact of M2(IL-4) polarization on intracellular labile Zn^{2+} using isotope dilution studies. IL-4 amplified the $^{68}Zn^{2+}/^{64}Zn^{2+}$ ratio in infected human monocytes (Figure 7F). These data provide evidence that IL-4 modulates Zn homeostasis in vitro, in vivo, and in human monocytes. Collectively, MT3 and SLC30A4 establish a regulatory network that programs M2(IL-4) macrophages to augment labile Zn^{2+} stores, culminating in a permissive environment for Zn acquisition by intracellular pathogens.

DISCUSSION

Classical and alternative activation create phenotypically and functionally distinct macrophage subsets. Alternatively activated macrophages constitute distinct populations such as M2(IL-4), M2(IL-13), and M2(IL-10), depending upon the stimulus received (Murray et al., 2014). For example, macrophage polarization by the Th2 cytokine IL-4 or IL-13 differentiates them into M2(IL-4) or M2(IL-13), respectively. Much is known about the functions of macrophages polarized by IL-4 or IL-13, but the mechanisms that drive their defense behavior remain elusive. In this study, we explored the Zn biology of M2 macrophages generated by IL-4 stimulation and its impact on the host response to intracellular infection. Our findings uncover a fundamental Zn-homeostatic MT3-SLC30A4 response that enriches the host labile Zn^{2+} stores and serves as a Zn resource for metal nourishment of an intracellular fungal pathogen.

GM-CSF signaling triggers MT1 and MT2 in macrophages via STAT5 and STAT3 (Subramanian Vignesh et al., 2013a). M2 polarization by IL-4 or IL-13 induced MT3, but not MT1 and MT2 and augmented intracellular Zn^{2+}. IL-4 and IL-13 share the IL-4Rα chain that signals via STAT6 and IRF4, while IL-10 and IL-33 signal via STAT3 and MyD88 pathways, respectively. Our observations indicate that macrophage Zn homeostasis not only diverges with the nature of the polarization signals, but also the signaling pathways mediated by them.

Regulation of metal homeostasis in phagocytes has a profound impact on shaping the fate of host-pathogen interactions (Hood and Skaar, 2012; Subramanian Vignesh et al., 2013b). Macrophage activation by GM-CSF restricts Zn by sequestration through MT1 and MT2 and functions as a major antifungal defense mechanism (Subramanian Vignesh et al., 2013a). M2(IL-4) macrophages, on the other hand, facilitate wound healing and collagen biosynthesis but poorly defend intracellular infections. A hallmark of M2 polarization by IL-4 is the production of arginase-1 that depletes NO and may facilitate the survival of pathogens that succumb to this reactive species (Mosser, 2003). However, NO-independent killing mechanisms exist (Newman and Gootee, 1992), suggesting that pathogens may be armed with alternative strategies to establish a niche within macrophages. Studies on metal regulation in M2 macrophages have focused on Fe metabolism. IL-4 induces the Fe storage protein ferritin and enhances transcription of the transferrin receptor (Weiss et al., 1997). Our data illustrate that in primary macrophages, IL-4 moderately enhanced total Zn import and selectively augmented labile Zn^{2+}, while total Fe remained unaltered. This behavior of M2 macrophages contrasts with proinflammatory activation by GM-CSF, whereby cells import a large amount of Zn for defense functions, but shield it from the exchangeable Zn^{2+} pool by sequestration.

Whereas MT1 and MT2 are ubiquitously expressed, MT3 is regarded as a brain-specific isoform, with neuronal growth inhibitory functions (Ding et al., 2010). We document that MT3 is expressed in the innate immune compartment, is strongly induced in M2 macrophages, and has a profound role in shaping Zn homeostasis in both the host and the pathogen. IL-4 and IL-13 expanded the exchangeable Zn^{2+} fraction in macrophages, thus making it readily bioavailable for exploitation by intracellular fungi. The nature of regulation of Zn homeostasis by M2 cytokines as opposed to GM-CSF illuminates distinct Zn regulatory profiles in proinflammatory versus anti-inflammatory macrophage activation states. Importantly, MT3 increased the intracellular labile Zn^{2+} stores independent of MT1 and MT2. This effect contrasts with the latter MTs that sequester the metal and only readily yield 1 Zn^{2+} (Jacob et al., 1998). Likewise, MT3 exhibits Zn donating properties distinct from its counterparts and releases Zn^{2+} under neuronal oxidative stress (Lee and Koh, 2010). In agreement with the structural peculiarity of the MT3 isoform that enables Zn^{2+} release, MT3 expanded the labile Zn^{2+} reservoir of M2(IL-4) macrophages.

Whether MT3 releases bound Zn or mobilizes it from storage organelles is unclear. We designed cathepsin activity and double isotope dilution studies to dissect Zn traffic and the origin of an augmented Zn^{2+} pool. Our data indicate a central role for aspartic and cysteine cathepsin proteases in shaping the phagocyte metal environment, specifically Zn^{2+} homeostasis. Cathepsins form a fundamental component of the cellular proteolytic machinery, and their activity is induced in macrophages under pathological conditions, including tumor formation and infection (Gocheva et al., 2010). In models of *S. aureus* and *M. tuberculosis* infection, induction of cathepsins in macrophages is associated with improved bacterial clearance (Müller et al., 2014; Rivera-Marrero et al., 2004). Our data demonstrate that by inducing Zn^{2+} release from MT3 under acidic conditions, cathepsins modulate the availability of a shared Zn^{2+} pool between host and the invading pathogen.

The elevation in intracellular labile $^{68}Zn^{2+}$ and accrual of ^{68}Zn by fungi clearly elucidates that M2(IL-4) macrophages derive ^{68}Zn from extracellular space and that MT3 and cathepsins "supply" Zn^{2+} in the labile form for exploitation by fungi. Determination of labile $^{68}Zn^{2+}/^{64}Zn^{2+}$ ratios revealed that resting-infected macrophages increased labile Zn^{2+}, albeit lower than in M2(IL-4) macrophages. This change was detected only by ^{68}Zn trafficking studies, suggesting that isotope enrichment enables identification of minute changes in labile Zn^{2+} by reducing the background signal from unlabeled Zn sources and only exhibiting the imported Zn pool. Thus, macrophage polarization with IL-4 potentiates availability of labile Zn^{2+} in the host that is assimilated by fungi. In contrast, GM-CSF not only limited Zn uptake by yeasts, but the fungus lost inherent ^{66}Zn to macrophages via sequestration in the MT peak. SLC39A2 is a major Zn importer in proinflammatory macrophages. In M2(IL-4) macrophages, this importer was not induced, but it partially contributed to intracellular $^{68}Zn^{2+}$ stores. The small but consistent induction of SLC39A6 and SLC39A12 may potentially

contribute to the labile Zn^{2+} pool. Contrary to the SLC39A2-dominant Zn influx mechanism in proinflammatory macrophages, our data suggest that labile Zn^{2+} is driven by multiple importers into M2(IL-4) macrophages. Zinpyr-1 revealed ubiquitous distribution of labile Zn^{2+} in M2(IL-4) macrophages. Access of this pool to yeasts may be facilitated by phagolysosomal Zn transporters (Hennigar and Kelleher, 2015). Acquisition of host ^{68}Zn by fungi in M2(IL-4) macrophages and fungal ^{66}Zn deprivation in response to GM-CSF indicates that Zn is shuttled across phagolysosomes in infected cells. The transporters that exchange Zn across phagolysosomes in response to M2 versus M1 stimuli, and how they shape microbial "accessibility" to the host Zn milieu is unknown.

SLC30A4 is distributed along the Golgi, endosomal, and mitochondrial membranes (McCormick and Kelleher, 2012; Palmiter and Huang, 2004). Thus, the spatial localization of SLC30A4 is governed by molecular cues that regulate Zn redistribution. SLC30A4 deficiency could redistribute labile Zn^{2+}, leading to binding of the free metal by other proteins, resulting in constriction of the labile Zn^{2+} pool. Although the transporter localized to phagolysosomes, Zn acquisition by the pathogen remained intact. Thus, compensatory mechanisms may operate to counter loss of SLC30A4. These may involve downregulation of a phagolysosomal Zn importer (import to cytosol) to conserve intra-organelle Zn stores or assimilation of the metal from Zn-bound proteins.

We extended the significance of our findings by establishing that IL-4 induced changes in Zn homeostasis in vivo and in human monocytes. Macrophages from both peritoneal exudate and lungs of infected mice mounted a Zn-homeostatic response to IL-4 comparable with primary bone marrow-derived macrophages. In vivo, peritoneal and pulmonary adoptive transfer of macrophages deficient in MT3 restrained fungal growth despite repeated exposure to IL-4. The influence of proinflammatory signals triggered by infection in vivo and an intracellular constricted free Zn^{2+} pool caused by MT3 deficiency may render intracellular yeasts susceptible to killing by these macrophages, even in the presence of an M2 signal. Indeed, despite macrophage polarization with IFN-γ, IL-4 favored the persistence of *H. capsulatum in* vitro, an effect that was compromised when MT3 was deficient. Type 2 immune responses drive elevated IL-4 and IL-13 production that dampen host resistance to intracellular infections. Moreover, Zn deficiency negatively influences IL-4 signaling (Gruber et al., 2013). Macrophages safeguard the host pathogen interface and possess a versatile defense arsenal, whose efficacy is reinforced by the polarization state. On the other hand, bacterial and fungal pathogens have evolved sophisticated mechanisms to combat host Zn limitation. The ZnuABC transporter arms *Salmonella typhimurium* to compete against Zn chelation by calprotectin. *C. albicans* secretes a zincophore designed to scavenge host Zn (Citiulo et al., 2012; Liu et al., 2012). From the pathogen standpoint, M2(IL-4) macrophages serve as a Zn-replete niche that is harnessed from the host during intracellular invasion. Manipulation of the M1 activation state by *Mycobacterium tuberculosis* (Harris et al., 2007), and preferential survival of *H. capsulatum* within the M2 subset are reminiscent of a favorable growth environment and disrupted intracellular antimicrobial defenses of this subset. Nonetheless, M2 polarization is central in parasite clearance and whether MT3 and SLC30A4 equip the M2 arsenal to fight this class of pathogens remains to be explored.

In summary, we have uncovered an MT3 and SLC30A4 driven nexus that shapes Zn metabolism as a dimension of M2 polarization to suppress host immunity. M2 signals lead macrophages to operate as a "Zn^{2+} harbor" whereby intracellular pathogens consume the metal at the expense of the host's readily exchangeable Zn^{2+} reservoir. Our data shed light on previously unidentified mechanisms that directly oppose nutritional immunity to permit microbial parasitization of macrophage metal resources. The finding that the brain-specific MT isoform MT3 has a fundamental role in the innate compartment has implications in understanding MT3 functions in shaping the immune response in M2-related pathologies. Thus, IL-4-driven macrophage polarization to the M2 phenotype triggers a Zn-homeostatic response to regulate macrophage effector functions that control host-pathogen interactions.

EXPERIMENTAL PROCEDURES

See also Supplemental Experimental Procedures.

Mice

C57BL/6 WT and *Ccr2*$^{-/-}$ mice were from Jackson Laboratory. *Stat6*$^{-/-}$ and *Irf4*$^{-/-}$ mice were gifts from Dr. Tim Eubank (The Ohio State University) and Dr. Lu Runqing (University of Nebraska Medical Center). Animals were maintained by the Department of Laboratory Animal Medicine, University of Cincinnati, accredited by the American Association for Accreditation of Laboratory Animal Care (Frederick, MD), and experiments were in accordance with Animal Welfare Act guidelines of the NIH.

Macrophages

Bone marrow macrophages were cultured with 10 ng/ml cytokine for 24 hr. Medium was replaced and cells were stimulated with cytokine and infected with five yeasts per macrophage for 24 hr prior to gene expression and metal analysis. For silencing, cells were treated with siRNA for 24 hr and 10 ng/ml cytokine for next 24 hr. Medium was replaced and cells were treated with cytokines and yeasts. After 24 hr, cells were used for SEC-ICP-MS or PCR. Lysates for SEC-ICP-MS were prepared in 0.1% SDS, yeasts were harvested, and cell lysates were passed through a 0.22 μm filter and frozen at $-80^{\circ}C$.

Silencing

Gene silencing was performed using siRNA complexed with TransIT TKO transfection reagent (Mirus) as per manufacturer's instructions (Subramanian Vignesh et al., 2013a). Cells were treated with siRNA for 24 hr, and cytokines were added for the next 24 hr. For infection, medium was replaced, and macrophages were stimulated with cytokines and infected with five yeasts per macrophage. Silencing was assessed 48–72 hr post-transfection.

Flow Cytometry

Cells were stained with CD11b, F4/80 (BD Biosciences), and CD45.1 (BioLegend) antibodies using standard protocols and run on Accuri C6 (BD Biosciences). Data were analyzed using FCS Express 4 (De Novo Software).

SEC-ICP-MS-MS

SEC-ICP-MS-MS was performed on cell lysates using an Agilent 1100 HPLC coupled to the ICP-MS-MS nebulizer. A TSK gel 3000SW was used for gel filtration, and a Superdex peptide column was used for CTSD activity assays. An Agilent 8800x ICP-MS was used in the MS/MS oxygen reaction mode for

detection of the ^{32}S isotope of sulfur by reacting it with oxygen. Total elemental analysis in macrophages and yeasts was performed by ICP-MS-MS after acid digestion via external calibration.

Microscopy

For confocal imaging, macrophages were plated on Millicell four-well glass EZ slides (Millipore) and treated as described above. Labile Zn was imaged 24 hr post-infection using Zinpyr-1 (Santa Cruz). Where indicated, cells were probed with SLC30A4 (Sigma) and LAMP1 (Abcam) antibodies. Images were acquired on a Zeiss LSM710 confocal microscope and visualized using ZEN 2011 software. MFI was analyzed using ImageJ.

Cathepsin Assay

MT3 was synthesized (GenScript) and purified using gel filtration chromatography. Low-, medium-, and high-^{68}Zn MT3 saturation forms were obtained by incubating reduced MT3 protein with different concentrations of ^{68}Zn to yield one, three, and six ^{68}Zn MT3 saturation forms. These forms were incubated with CTSD in pH 5.5, 6.5, and 7.5 buffers for 3 hr at 37°C. MT3 degradation and Zn^{2+} release were assessed by monitoring sulfur and Zn signals in the MT3 peak and at low molecular mass.

Double Isotope Dilution

RPMI and HAM'S F12 yeast growth media containing ^{68}Zn and ^{66}Zn, respectively, were made. Macrophages were plated in ^{68}Zn RPMI media, treated with cytokines and infected with ^{66}Zn *H. capsulatum*. ^{66}Zn yeasts were obtained by more than ten passages in ^{66}Zn HAM'S F12. Cells were harvested for SEC-ICP-MS-MS, and ^{68}Zn and ^{66}Zn signals were monitored for ^{68}Zn flux into cells, acquisition of ^{68}Zn by yeasts in M2(IL-4) macrophages, and loss of yeast-^{66}Zn by sequestration in GM-CSF-activated macrophages. ^{68}Zn and ^{66}Zn were compared with respect to ^{64}Zn that retained natural abundance.

In Vivo and Human Monocytes

Mice were treated i.p. with IL-4 and infected with 2×10^6 GFP^+ yeasts. Peritoneal macrophages were isolated for flow cytometry and gene expression studies. WT and *Ccr2*$^{-/-}$ mice were infected i.n., and $F4/80^+CD11b^+$ macrophages were sorted from lung leukocytes for gene expression analysis. Human monocytes (Hoxworth Blood Center) were obtained from peripheral blood mononuclear cells from five donors, stimulated with IL-4, and infected to assess Zn distribution. Human studies were approved by institutional review board at the University of Cincinnati.

Statistical Analysis

p values were calculated by one-way ANOVA for multiple comparisons using Holm Sidak, Tukey, or Bonferroni methods using three or more replicates, and non-paired Student's t test was used to compare two groups (*$p < 0.05$, **$p < 0.01$, and ##$p < 0.001$; NS, not significant, ND, not detected).

SUPPLEMENTAL INFORMATION

Supplemental Information includes Supplemental Experimental Procedures, five figures, and one table and can be found with this article online at http://dx.doi.org/10.1016/j.celrep.2016.08.057.

AUTHOR CONTRIBUTIONS

K.S.V. wrote the manuscript. K.S.V. and J.A.L.F. designed and performed experiments. K.S.V. did microscopic, molecular, flow cytometry, in vitro, in vivo, and human experiments and interpreted data. J.A.L.F. did chromatographic separations with UV-Vis, ICP-MS, and ESI-IT-MS-MS detection, total elemental analysis, and bottoms-up proteomics and interpreted data. A.P. performed bioinformatics. S.D., J.A.C., and G.S.D. supervised the work.

ACKNOWLEDGMENTS

This work is dedicated to the memory of Professor Dr. Joseph A. Caruso, whose contributions to this work are inestimable. This work was supported by NIH grants AI106269 (G.S.D.) and DK099222 (S.D.). K.S.V. is supported by American Heart Association grant 15POST25700182, 2015, and Center for Environmental Genetics, National Institute for Environmental Health Sciences, grant P30ES006096. We thank Agilent Technologies for LCMS and 8800 ICP-MS-MS support, Dr. A. Verma for technical assistance, and Drs. S. Newman and B. S. Klein for valuable suggestions. Proteomic data are provided in the Supplemental Information.

Received: March 17, 2016
Revised: July 18, 2016
Accepted: August 17, 2016
Published: September 20, 2016

REFERENCES

Allendoerfer, R., and Deepe, G.S., Jr. (1997). Intrapulmonary response to *Histoplasma capsulatum* in gamma interferon knockout mice. Infect. Immun. *65*, 2564–2569.

Balce, D.R., Li, B., Allan, E.R., Rybicka, J.M., Krohn, R.M., and Yates, R.M. (2011). Alternative activation of macrophages by IL-4 enhances the proteolytic capacity of their phagosomes through synergistic mechanisms. Blood *118*, 4199–4208.

Citiulo, F., Jacobsen, I.D., Miramón, P., Schild, L., Brunke, S., Zipfel, P., Brock, M., Hube, B., and Wilson, D. (2012). *Candida albicans* scavenges host zinc via Pra1 during endothelial invasion. PLoS Pathog. *8*, e1002777.

Ding, Z.C., Ni, F.Y., and Huang, Z.X. (2010). Neuronal growth-inhibitory factor (metallothionein-3): structure-function relationships. FEBS J. *277*, 2912–2920.

El Chartouni, C., Schwarzfischer, L., and Rehli, M. (2010). Interleukin-4 induced interferon regulatory factor (Irf) 4 participates in the regulation of alternative macrophage priming. Immunobiology *215*, 821–825.

Figueroa, J.A., Vignesh, K.S., Deepe, G.S., Jr., and Caruso, J. (2014). Selectivity and specificity of small molecule fluorescent dyes/probes used for the detection of Zn^{2+} and Ca^{2+} in cells. Metallomics *6*, 301–315.

Gocheva, V., Wang, H.W., Gadea, B.B., Shree, T., Hunter, K.E., Garfall, A.L., Berman, T., and Joyce, J.A. (2010). IL-4 induces cathepsin protease activity in tumor-associated macrophages to promote cancer growth and invasion. Genes Dev. *24*, 241–255.

Gruber, K., Maywald, M., Rosenkranz, E., Haase, H., Plumakers, B., and Rink, L. (2013). Zinc deficiency adversely influences interleukin-4 and interleukin-6 signaling. J. Biol. Regul. Homeost. Agents *27*, 661–671.

Haase, H., and Rink, L. (2014). Zinc signals and immune function. Biofactors *40*, 27–40.

Haase, H., Ober-Blöbaum, J.L., Engelhardt, G., Hebel, S., Heit, A., Heine, H., and Rink, L. (2008). Zinc signals are essential for lipopolysaccharide-induced signal transduction in monocytes. J. Immunol. *181*, 6491–6502.

Harris, J., De Haro, S.A., Master, S.S., Keane, J., Roberts, E.A., Delgado, M., and Deretic, V. (2007). T helper 2 cytokines inhibit autophagic control of intracellular Mycobacterium tuberculosis. Immunity *27*, 505–517.

Hennigar, S.R., and Kelleher, S.L. (2015). TNFα Post-Translationally Targets ZnT2 to Accumulate Zinc in Lysosomes. J. Cell. Physiol. *230*, 2345–2350.

Hood, M.I., and Skaar, E.P. (2012). Nutritional immunity: transition metals at the pathogen-host interface. Nat. Rev. Microbiol. *10*, 525–537.

Jacob, C., Maret, W., and Vallee, B.L. (1998). Control of zinc transfer between thionein, metallothionein, and zinc proteins. Proc. Natl. Acad. Sci. U S A *95*, 3489–3494.

Kahnert, A., Seiler, P., Stein, M., Bandermann, S., Hahnke, K., Mollenkopf, H., and Kaufmann, S.H. (2006). Alternative activation deprives macrophages of a coordinated defense program to Mycobacterium tuberculosis. Eur. J. Immunol. *36*, 631–647.

Lee, S.J., and Koh, J.Y. (2010). Roles of zinc and metallothionein-3 in oxidative stress-induced lysosomal dysfunction, cell death, and autophagy in neurons and astrocytes. Mol. Brain *3*, 30.

Leopold Wager, C.M., and Wormley, F.L., Jr. (2014). Classical versus alternative macrophage activation: the Ying and the Yang in host defense against pulmonary fungal infections. Mucosal Immunol. *7*, 1023–1035.

Li, Y., and Maret, W. (2008). Human metallothionein metallomics. J. Anal. At. Spectrom. *23*, 1055–1062.

Liu, J.Z., Jellbauer, S., Poe, A.J., Ton, V., Pesciaroli, M., Kehl-Fie, T.E., Restrepo, N.A., Hosking, M.P., Edwards, R.A., Battistoni, A., et al. (2012). Zinc sequestration by the neutrophil protein calprotectin enhances *Salmonella* growth in the inflamed gut. Cell Host Microbe *11*, 227–239.

McCormick, N.H., and Kelleher, S.L. (2012). ZnT4 provides zinc to zinc-dependent proteins in the trans-Golgi network critical for cell function and Zn export in mammary epithelial cells. Am. J. Physiol. Cell Physiol. *303*, C291–C297.

McKim, J.M., Jr., Choudhuri, S., and Klaassen, C.D. (1992). In vitro degradation of apo-, zinc-, and cadmium-metallothionein by cathepsins B, C, and D. Toxicol. Appl. Pharmacol. *116*, 117–124.

Mosser, D.M. (2003). The many faces of macrophage activation. J. Leukoc. Biol. *73*, 209–212.

Mosser, D.M., and Edwards, J.P. (2008). Exploring the full spectrum of macrophage activation. Nat. Rev. Immunol. *8*, 958–969.

Müller, S., Faulhaber, A., Sieber, C., Pfeifer, D., Hochberg, T., Gansz, M., Deshmukh, S.D., Dauth, S., Brix, K., Saftig, P., et al. (2014). The endolysosomal cysteine cathepsins L and K are involved in macrophage-mediated clearance of Staphylococcus aureus and the concomitant cytokine induction. FASEB J. *28*, 162–175.

Murray, P.J., Allen, J.E., Biswas, S.K., Fisher, E.A., Gilroy, D.W., Goerdt, S., Gordon, S., Hamilton, J.A., Ivashkiv, L.B., Lawrence, T., et al. (2014). Macrophage activation and polarization: nomenclature and experimental guidelines. Immunity *41*, 14–20.

Newman, S.L., and Gootee, L. (1992). Colony-stimulating factors activate human macrophages to inhibit intracellular growth of *Histoplasma capsulatum* yeasts. Infect. Immun. *60*, 4593–4597.

Palmiter, R.D., and Huang, L. (2004). Efflux and compartmentalization of zinc by members of the SLC30 family of solute carriers. Pflugers Arch. *447*, 744–751.

Rivera-Marrero, C.A., Stewart, J., Shafer, W.M., and Roman, J. (2004). The down-regulation of cathepsin G in THP-1 monocytes after infection with Mycobacterium tuberculosis is associated with increased intracellular survival of bacilli. Infect. Immun. *72*, 5712–5721.

Subramanian Vignesh, K., and Deepe, G.S., Jr. (2016). Immunological orchestration of zinc homeostasis: The battle between host mechanisms and pathogen defenses. Arch. Biochem. Biophys. Published online February 4, 2016. http://dx.doi.org/10.1016/j.abb.2016.02.020.

Subramanian Vignesh, K., Landero Figueroa, J.A., Porollo, A., Caruso, J.A., and Deepe, G.S., Jr. (2013a). Granulocyte macrophage-colony stimulating factor induced Zn sequestration enhances macrophage superoxide and limits intracellular pathogen survival. Immunity *39*, 697–710.

Subramanian Vignesh, K., Landero Figueroa, J.A., Porollo, A., Caruso, J.A., and Deepe, G.S., Jr. (2013b). Zinc sequestration: arming phagocyte defense against fungal attack. PLoS Pathog. *9*, e1003815.

Szymczak, W.A., and Deepe, G.S., Jr. (2009). The CCL7-CCL2-CCR2 axis regulates IL-4 production in lungs and fungal immunity. J. Immunol. *183*, 1964–1974.

Teigelkamp, S., Bhardwaj, R.S., Roth, J., Meinardus-Hager, G., Karas, M., and Sorg, C. (1991). Calcium-dependent complex assembly of the myeloic differentiation proteins MRP-8 and MRP-14. J. Biol. Chem. *266*, 13462–13467.

Verma, A., Kroetz, D.N., Tweedle, J.L., and Deepe, G.S., Jr. (2015). Type II cytokines impair host defense against an intracellular fungal pathogen by amplifying macrophage generation of IL-33. Mucosal Immunol. *8*, 380–389.

Weiss, G., Bogdan, C., and Hentze, M.W. (1997). Pathways for the regulation of macrophage iron metabolism by the anti-inflammatory cytokines IL-4 and IL-13. J. Immunol. *158*, 420–425.